WILEY

Numerical convergence of nonlinear nonlocal continuum models to local elastodynamics

Prashant K. Jha[iD] | Robert Lipton[iD]

Department of Mathematics, Louisiana State University, Baton Rouge, Louisiana, USA

Correspondence
Robert Lipton, Department of Mathematics, 303 Lockett Hall, Louisiana State University, Baton Rouge, LA 70803-4918 USA.
Email: lipton@math.lsu.edu

Summary

We quantify the numerical error and modeling error associated with replacing a nonlinear nonlocal bond-based peridynamic model with a local elasticity model or a linearized peridynamic model away from the fracture set. The nonlocal model treated here is characterized by a double-well potential and is a smooth version of the peridynamic model introduced in the work of Silling. The nonlinear peridynamic evolutions are shown to converge to the solution of linear elastodynamics at a rate linear with respect to the length scale ϵ of nonlocal interaction. This rate also holds for the convergence of solutions of the linearized peridynamic model to the solution of the local elastodynamic model. For local linear Lagrange interpolation, the consistency error for the numerical approximation is found to depend on the ratio between mesh size h and ϵ. More generally, for local Lagrange interpolation of order $p \geq 1$, the consistency error is of order h^p/ϵ. A new stability theory for the time discretization is provided and an explicit generalization of the CFL condition on the time step and its relation to mesh size h is given. Numerical simulations are provided illustrating the consistency error associated with the convergence of nonlinear and linearized peridynamics to linear elastodynamics.

KEYWORDS

finite element approximation, nonlocal mechanics, numerical analysis, peridynamic modeling

1 | INTRODUCTION

The nonlocal formulation proposed in the work of Silling[1] provides a framework for modeling crack propagation inside solids. The basic idea is to redefine the strain in terms of the difference quotients of the displacement field and allow for nonlocal forces acting within a finite horizon. The relative size of the horizon with respect to the diameter of the domain of the specimen is denoted by ϵ. The force at any given material point is determined by the deformation of all neighboring material points surrounding it within a radius given by the size of horizon. Computational fracture modeling using peridynamics features formation and evolution of interfaces associated with fracture, see other works.[2-15]

In the absence of fracture, earlier work demonstrates the convergence of linear peridynamic models to the local model of linear elasticity as ϵ goes to zero, see the works of Weckner and Emmrich[16] and Silling and Lehoucq.[17] The convergence of an equilibrium peridynamic model to the Navier equation in the sense of solution operators is established in the work of Mengesha and Du.[18] Numerical analysis of linear peridynamic models for one-dimensional (1D) bars have been given in

the work of Bobaru et al[8] and Weckner and Emmrich.[16] Related approximations of nonlocal diffusion models are discussed in the works of Tian et al,[19] Chen and Gunzburger,[20] and Du et al.[21] A stability analysis of the numerical approximation to solutions of linear nonlocal wave equations is given in the work of Guan and Gunzburger.[22]

In this work, we analyze the discrete approximations to the nonlinear nonlocal model developed in the works of Lipton.[23,24] This model is a smooth version of the prototypical micro-elastic model introduced in the work of Silling,[1] see Section 2. In earlier theoretical work, it has been shown that, in the limit of vanishing nonlocality, this model delivers evolutions possessing sharp displacement discontinuities associated with cracks. The limiting displacement field evolution has bounded Griffith fracture energy and away from the fracture set satisfies classic local elastodynamics.[23-25] This model motivates adaptive implementations of peridynamics for brittle fracture. In regions of the body where brittle fracture is anticipated, one would apply the nonlinear nonlocal model, but in regions where no fracture is to be anticipated, one would like to apply the linear elastic model. In this paper, we will assume that the solution is differentiable and there is no fracture. Here, we investigate the difference between numerically computed solutions for the nonlinear nonlocal bond-based model with those of the linearized nonlocal model and those of classic local elastodynamics. The types of nonlocal kernels associated with these prototypical models are central to the theory but up until now have not been treated in the literature.

In this work, we show that the solutions of the nonlinear model converge to classical elastodynamics at a rate that is linear in ϵ. We analyze the numerical approximation associated with linear interpolation in space for two cases: (i) when the size of horizon is fixed and the mesh size h tends to zero, known as h-convergence, and (ii) when the size of the horizon also tends to zero and the mesh approaches zero faster than the horizon. For the first case, we show that consistency error is of order $O(\frac{h}{\epsilon})$ for both nonlinear and linearized models, see Proposition 2. For the second case, we find that the consistency error for both models is $O(\frac{h}{\epsilon}) + O(\epsilon)$, see Proposition 3. These ideas are easily extended to higher-order local Lagrange interpolation. For pth order local polynomial interpolations $p \geq 1$, the consistency error for both models and case (i) is of order $O(h^p/\epsilon)$ and for both models and case (ii) is of order $O(h^p/\epsilon) + O(\epsilon)$, see Propositions 4 and 5. These results show that the grid refinement relative to the horizon length scale has more importance than decreasing the horizon length when establishing convergence to the classical elastodynamics description.

Earlier related work[25] analyzes the nonlinear model and establishes the existence of nondifferentiable Hölder continuous solutions. It is shown there that the rate of convergence of the discrete model to the continuum nonlocal model is of the order h^γ/ϵ, where $0 < \gamma \leq 1$ is the Hölder exponent. The work presented here shows that we can improve the rate of convergence for this model if we have a priori knowledge on the number of bounded continuous derivatives of the solution. In this paper, we have restricted the analysis and simulations to the 1D case to illustrate the ideas. For higher-dimensional problems, the convergence rates are the same, see Section 6, and future work will address the consistency error in higher dimensions using the same techniques developed here.

A second issue is the coordination of spatial and temporal discretization to insure stability for numerical approximation of nonlocal models. Here, the stability for the central difference in time approximation to the linearized model is considered. Analysis of the linearized peridynamic nonlocal model shows that the stability is given by a new explicit condition that converges to the well-known CFL condition as $\epsilon \to 0$, see Theorem 3. One no longer has an explicit stability condition for the nonlinear model. However, it is found that the semidiscrete approximation of the nonlinear model is stable in the energy norm, see our other work.[25]

In Section 5, we present numerical simulations that confirm the error estimates for both linearized and nonlinear peridynamics. The numerical experiments show that the discretization error can be reduced by choosing the ratio h/ϵ suitably small for every choice of ϵ as $\epsilon \to 0$, see Figure 4. We verify the convergence rates by simulating the peridynamic model long enough to include the boundary effects due to wave reflection in Section 5.1. Our numerical studies confirm that the solutions of linear and nonlinear peridynamics are indistinguishable for sufficiently small horizon ϵ.

The analysis of mechanical and mathematical aspects of peridynamic models different than those treated here can be found in other works.[9,10,26-31] A full accounting of the peridynamics literature lies beyond the scope of this paper; however, several themes and applications are covered in the recent handbook.[32]

The organization of this paper is as follows. In Section 2, we introduce the class of nonlocal nonlinear potentials and describe the convergence of peridynamic models to classical elastodynamics. In Section 3, we introduce the finite element approximation of the model and present bounds on the discretization error. In Section 4, we consider the central difference in time scheme and obtain the stability condition on Δt as function of ϵ and h. In Section 5, we present the numerical simulations. In Section 6, we present the convergence of the model in higher dimensions. The proofs of the theorems are given in Section 7, and we provide our conclusions in Section 8.

2 | NONLOCAL EVOLUTION AND ELASTODYNAMICS

The mathematical formulation for the nonlocal model is presented in this section. We exhibit the convergence rate of nonlocal solutions to the solution to linear elastodynamics in the limit of vanishing peridynamic horizon. A convergence rate is also provided for the linearized nonlocal model. The convergence rate for the nonlocal kernels treated here has not been addressed before in the literature.

2.1 | The nonlocal model

We consider the nonlocal potentials introduced in the works of Lipton.[23,24] Let $D := [a, b] \subset \mathbb{R}$ be a bounded material domain in one dimension and $J = [0, T]$ be an interval of time. The nonlocal boundary denoted by ∂D^ϵ is intervals of diameter 2ϵ on either side of D and given by $(a - \epsilon, a + \epsilon) \cup (b - \epsilon, b + \epsilon)$. The strain S for the 1D peridynamic model is given by the difference quotient

$$S(y, x; u) := \frac{u(y) - u(x)}{|y - x|}.$$

The nonlocal force is given in terms of the nonlinear two-point interaction potential W^ϵ defined by

$$W^\epsilon(S, y - x) = \frac{2J^\epsilon(|y - x|)}{\epsilon|y - x|} f\left(|y - x|S^2\right),$$

where $f : r \in \mathbb{R}^+ \to \mathbb{R}$ is positive, smooth, and concave with following properties:

$$\lim_{r \to 0^+} \frac{f(r)}{r} = f'(0) \qquad \text{and} \qquad \lim_{r \to \infty} f(r) = f_\infty < \infty. \tag{1}$$

The potential $W^\epsilon(S, y - x)$ is of double-well type and convex near the origin, where it has one well, the second well is at ∞ and associated with the horizontal asymptote $W^\epsilon(\infty, y - x)$, see Figure 1. The function $J^\epsilon(|y - x|)$ influences the magnitude of the nonlocal force due to y on x. We define J^ϵ by rescaling $J(|\xi|)$, ie, $J^\epsilon(|\xi|) = J(|\xi|/\epsilon)$. The influence function J is zero outside the ball $[-1, 1]$ and satisfies $0 \leq J(|\xi|) \leq M$ for all $\xi \in [-1, 1]$.

The force of two-point interaction between x and y is derived from the nonlocal potential and given by $\partial_S W^\epsilon(S, y - x)$, see Figure 2. For small strains, the force is linear and elastic and then softens as the strain becomes larger. The critical
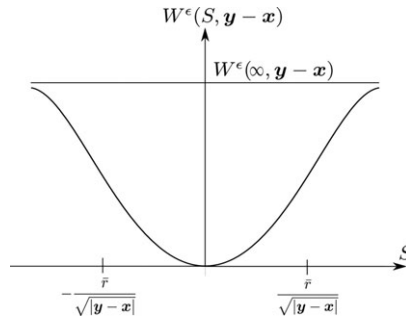
FIGURE 1 Two-point potential $W^\epsilon(S, y - x)$ as a function of strain S for fixed $y - x$
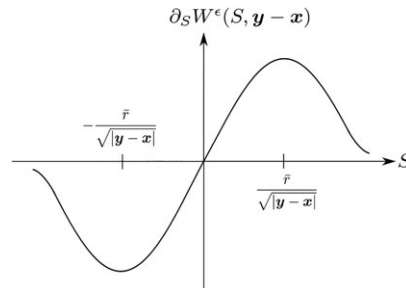
FIGURE 2 Nonlocal force $\partial_S W^\epsilon(S, y - x)$ as a function of strain S for fixed $y - x$. Second derivative of $W^\epsilon(S, y - x)$ is zero for $S = S_c := \pm\bar{r}/\sqrt{|y - x|}$
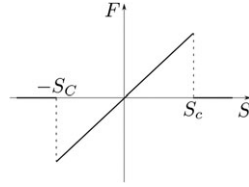
FIGURE 3 Prototypical micro-elastic bond model in the work of Silling[1] as a function of strain S for fixed $y - x$. Here, the nonlocal force drops to zero at $S = S_c$

strain, for which the force between x and y begins to soften, is given by $S_c(y, x) := \bar{r}/\sqrt{|y - x|}$ and the force decreases monotonically for

$$|S(y, x; u)| > S_c.$$

Here, $\bar{r}$ is the inflection point of $r : \to f(r^2)$ and is the root of following equation:

$$f'(r^2) + 2r^2 f''(r^2) = 0.$$

The nonlocal force $-\nabla PD^\epsilon$ is defined by

$$-\nabla PD^\epsilon(u)(x) = \frac{1}{2\epsilon} \int_{x-\epsilon}^{x+\epsilon} \partial_S W^\epsilon(S, y - x) dy$$

$$= \frac{2}{\epsilon^2} \int_{x-\epsilon}^{x+\epsilon} J(|y - x|/\epsilon) f'\left(|y - x| S(y, x; u)^2\right) S(y, x; u) dy.$$

This force-strain model is a smooth version of the prototypical micro-elastic model,[1] which exhibits an abrupt drop in the force after a critical strain, see Figure 3.

Similarly, we denote $-\nabla PD_l^\epsilon(u)(x)$ as the linearized peridynamic force at x, given by

$$-\nabla PD_l^\epsilon(u)(x) = \frac{2}{\epsilon^2} \int_{x-\epsilon}^{x+\epsilon} J(|y - x|/\epsilon) f'(0) S(y, x; u) dy.$$

The corresponding linearized local model is characterized by the Young's modulus $\mathbb{C}$ given by

$$
\begin{aligned}
\mathbb{C} &= \int_{-1}^{1} J(|z|) f'(0) |z| dz \\
&= \frac{1}{\epsilon^2} \int_{x-\epsilon}^{x+\epsilon} J(|y - x|/\epsilon) f'(0) |y - x| dy, \qquad \forall x, \epsilon > 0.
\end{aligned}
\tag{2}
$$

2.2 | The dynamic evolution

We now state the initial boundary problem for the three types of evolutions: the first is given by the nonlinear nonlocal model, the second is given by the linearized nonlocal model, and the third is given by the classic local linear elastic model. Let u^ϵ be the solution of the peridynamic equation of evolution, u_l^ϵ be the solution of the linearized peridynamic equation of evolution, and u be the solution of elastodynamic equation of evolution with Young's modulus $\mathbb{C}$. For comparison of u_l^ϵ and u^ϵ with u, we assume u to be extended by zero outside D. The displacements u^ϵ, u_l^ϵ, and u satisfy the following evolution equations, for all $(x, t) \in D \times J$, described by

$$\rho \ddot{u}(t, x) = \mathbb{C} u_{xx}(t, x) + b(t, x), \tag{3}$$

$$\rho \ddot{u}^\epsilon(t, x) = -\nabla PD^\epsilon(u^\epsilon(t))(x) + b(t, x), \tag{4}$$

$$\rho \ddot{u}_l^\epsilon(t, x) = -\nabla PD_l^\epsilon\left(u_l^\epsilon(t)\right)(x) + b(t, x), \tag{5}$$

where $b(t, x)$ is a prescribed body force and the mass density ρ is taken to be constant. The boundary conditions are given by

$$u^\epsilon(t, x) = 0 \quad \text{and} \quad \dot{u}^\epsilon(t, x) = 0, \quad \forall t \in J, \forall x \in \partial D^\epsilon,$$

and the same boundary conditions hold for u_l^ϵ and u. The initial condition is given by

$$u^\epsilon(0, x) = g(x) \quad \text{and} \quad \dot{u}^\epsilon(0, x) = h(x), \quad \forall x \in D,$$

with $g = h = 0$ outside some fixed subset D' of D. The same initial condition also holds for u_l^ϵ and u. For future reference, we denote the width of the layer $D \setminus D'$ by δ.

2.3 | Convergence of nonlocal models in the limit of vanishing horizon

In this section, we provide convergence rates that show that the solution u^ϵ of the peridynamic equation converges, in the limit $\epsilon \to 0$, to the solution u of the elastodynamic equation. The model treated here was considered earlier but for solutions that may not be differentiable and exhibit discontinuities.[23,24] Convergence was established for this case; however, no convergence rate is available. For linear nonlocal models with kernels different than the ones treated here, the limiting behavior has been identified by several investigators in the peridynamics literature, see other works.[17,28,30,33]

We first provide estimates for the difference between the peridynamics force, the linearized peridynamics force, and the elastodynamics force. With these estimates in hand, we then present the rate of convergence of the solution of the nonlinear nonlocal evolution to the solution of the local linear elastic wave equation. In what follows, $C^n(D)$ is the space of functions with n continuous derivatives on D.

Proposition 1. (Control on the difference between peridynamic force and local elastic force)
If $u \in C^3(D)$ and

$$\sup_{x \in D} |u_{xxx}(x)| < \infty,$$

then

$$\sup_{x \in D} \left| -\boldsymbol{\nabla}PD^\epsilon(u)(x) - \left(-\boldsymbol{\nabla}PD_l^\epsilon(u)(x) \right) \right| = O(\epsilon), \tag{6}$$

$$\sup_{x \in D} \left| -\boldsymbol{\nabla}PD_l^\epsilon(u)(x) - \mathbb{C}u_{xx}(x) \right| = O(\epsilon), \tag{7}$$

so

$$\sup_{x \in D} \left| -\boldsymbol{\nabla}PD^\epsilon(u)(x) - \mathbb{C}u_{xx}(x) \right| = O(\epsilon). \tag{8}$$

If $u \in C^4(D)$ and

$$\sup_{x \in D} |u_{xxxx}(x)| < \infty, \tag{9}$$

then

$$\sup_{x \in D} \left| -\boldsymbol{\nabla}PD_l^\epsilon(u)(x) - \mathbb{C}u_{xx}(x) \right| = O(\epsilon^2). \tag{10}$$

We introduce the usual $H^1(D)$ norm of a function f defined in D by

$$\|f\|_1 = \sqrt{\int_D |f(x)|^2 \, dx + \int_D |f_x(x)|^2 \, dx}.$$

We now state the theorem that shows that $u^\epsilon \to u$ with rate ϵ in the $H^1(D)$ norm uniformly in time.

Theorem 1. (Convergence of nonlinear peridynamics to the linear elastic wave equation in the limit that the horizon goes to zero)
Let $e^\epsilon := u^\epsilon - u$, where u^ϵ is the solution of Equation (4) and u is the solution of Equation (3). Suppose $u^\epsilon(t) \in C^4(D)$, for all $\epsilon > 0$ and $t \in [0, T]$. Suppose there exists $C_1 > 0$, C_1 independent of the size of horizon ϵ, such that

$$\sup_{\epsilon > 0} \left\{ \sup_{(x,t) \in D \times J} |u_{xxxx}^\epsilon(t, x)| \right\} < C_1 < \infty.$$

Then, for $\epsilon < \delta$, there is a constant $C_2 > 0$ independent of δ, ϵ, such that

$$\sup_{t\in[0,T]} \left\{ \int_D \rho|\dot{e}^\epsilon(t,x)|^2\mathrm{d}x + \int_D \mathbb{C}|e_x^\epsilon(t,x)|^2\mathrm{d}x \right\} \leq C_2\epsilon^2,$$

so $u^\epsilon \to u$ in the $H^1(D)$ norm at the rate ϵ uniformly in time $t \in [0, T]$.

A stronger convergence result holds for the solutions $u_l^\epsilon(t)$ of the family of linearized peridynamic equations.

Theorem 2. (Convergence of linearized peridynamics equation to the linear elastic wave equation in the limit that the horizon goes to zero)

Let $e_l^\epsilon := u_l^\epsilon - u$, where u_l^ϵ is the solution of Equation (5) and u is the solution of Equation (3). Suppose $u_l^\epsilon(t) \in C^4(D)$, for all $\epsilon > 0$ and $t \in [0, T]$. Suppose there exists $C_1 > 0$, C_1 independent of the size of horizon ϵ, such that

$$\sup_{\epsilon>0} \left\{ \sup_{(x,t)\in D\times J} \left|\left(u_l^\epsilon\right)_{xxxx}(t,x)\right| \right\} < C_1 < \infty.$$

Then, there is a constant $C_2 > 0$ independent of δ, ϵ, such that

$$\sup_{t\in[0,T]} \left\{ \int_D \rho\left|\dot{e}_l^\epsilon(t,x)\right|^2 \mathrm{d}x + \int_D \mathbb{C}\left|\left(e_l^\epsilon\right)_x(t,x)\right|^2 \mathrm{d}x \right\} \leq C_2\epsilon^4,$$

so $u_l^\epsilon \to u$ in the $H^1(D)$ norm at the rate ϵ^2 uniformly in time $t \in [0, T]$.

The proofs of Proposition 1 and Theorems 1 and 2 are given in Section 7. We now discuss the finite element approximation of the peridynamic model and show the consistency of the discretization for both piecewise constant and linear interpolation.

3 | DISCRETE APPROXIMATION

In this section, we introduce the spatial discretization for the peridynamics evolution. To introduce the ideas, we use a linear continuous interpolation over uniform mesh and write the equation of motion of displacement at the mesh points. This type of approximation has been analyzed in the work of Tian and Du[34] in the 1D setting and further extended to higher dimensions in the works Tian et al[19,35] for a significant class quasi-static problems with linear kernels different than the ones treated in this investigation.

Let h characterize the mesh size and be given by the distance between grid points. We let $\overline{D}$ and $\overline{\partial D^\epsilon}$ denote the closure of the sets D and ∂D^ϵ. To fix ideas, we will suppose that $\overline{D}$ and $\overline{\partial D^\epsilon}$ contain an integral number of elements of the mesh. Let $D_h = D \cap h\mathbb{Z}$ and $\partial D^{\epsilon,h} = \partial D^\epsilon \cap h\mathbb{Z}$, and let $K = \{i \in \mathbb{Z} : ih \in \overline{D}\}$ and $K_\epsilon = \{i \in \mathbb{Z} : ih \in \overline{\partial D^\epsilon}\}$. Here, K_ϵ corresponds to the list of nodes located inside the closure of the nonlocal boundary ∂D^ϵ. We assume $x_i = ih$. We define the interpolation operator $I_h[\cdot]$, for a given function $g : \overline{D \cup \partial D^\epsilon} \to \mathbb{R}$, as follows:

$$\mathcal{I}_h[g(y)] = \sum_{i\in K\cup K_\epsilon} g(x_i)\phi_i(y),$$

where $\phi_i(\cdot)$ is the interpolation function associated to the node i and $\{\phi_i\}_{i\in K\cup K_\epsilon}$ is a partition of unity, ie,

$$\sum_{i\in K\cup K_\epsilon} \phi_i(x) = 1$$

for all $x \in \overline{D \cup \partial D^\epsilon}$. In order to expedite the presentation, we assume that the diameter of nonlocal interaction 2ϵ is fixed and always contains an integral number of grid points $2m + 1$. For this choice, $\epsilon = mh$, where m increases as h decreases. When we investigate m convergence, we will allow both ϵ and h to decrease.

We also consider extensions of discrete sets defined on the nodes $K \cup K_\epsilon$. We write the function $v(t, x_i)$ defined at node x_i as $v_i(t)$ and define the discrete set $\{v_i(t)\}_{K \cup K_\epsilon}$. The function $\hat{u}_h^\epsilon(t)$ is the extension of discrete set $\{\hat{u}_i^\epsilon(t)\}_{K \cup K_\epsilon}$ using the interpolation functions and is defined by

$$\hat{u}_h^\epsilon(t) = E\left[\{\hat{u}_i^\epsilon(t)\}_{K \cup K_\epsilon}\right] = \sum_{i \in K \cup K_\epsilon} \hat{u}_i^\epsilon(t)\phi_i(x), \qquad \forall x \in \overline{D \cup \partial D^\epsilon}.$$

We also have the body force $b_h(t)$ given by the extension of discrete set $\{b_i(t)\}_{K \cup K_\epsilon}$ defined by

$$b_h(t) = E\left[\{b_i(t)\}_{K \cup K_\epsilon}\right] = \sum_{i \in K \cup K_\epsilon} b_i(t)\phi_i(x), \qquad \forall x \in \overline{D \cup \partial D^\epsilon}.$$

Let $\hat{u}_h^\epsilon(t)$ be the solution of following equation:

$$\rho \ddot{\hat{u}}_i^\epsilon(t) = -\nabla PD^\epsilon\left(\hat{u}_h^\epsilon(t)\right)(x_i) + b_i(t), \tag{11}$$

with initial condition defined at the nodes given by

$$\hat{u}_i^\epsilon(0) = f(x_i), \qquad \dot{\hat{u}}_i^\epsilon(0) = g(x_i), \qquad \forall i \in K,$$

or equivalently given by the extension of the discrete sets

$$\hat{u}_h^\epsilon(0) = f_h, \qquad \dot{\hat{u}}_h^\epsilon(0) = g_h, \qquad \forall i \in K, \tag{12}$$

and homogeneous boundary condition given by

$$\hat{u}_i^\epsilon(t) = 0, \qquad \dot{\hat{u}}_i^\epsilon(t) = 0, \qquad \forall i \in K_\epsilon. \tag{13}$$

Similarly, the discrete set $\{\hat{u}_{l,i}^\epsilon(t)\}_{i \in K \cup K_\epsilon}$, with subscript l, is extended by interpolation to the function $\hat{u}_{l,h}^\epsilon(t) = E[\{\hat{u}_{l,i}^\epsilon(t)\}_{i \in K \cup K_\epsilon}]$ and satisfies the linear peridynamic equation

$$\rho \ddot{\hat{u}}_{l,i}^\epsilon(t) = -\nabla PD_l^\epsilon\left(\hat{u}_{l,h}^\epsilon(t)\right)(x_i) + b_i(t)$$

$$= \frac{2}{\epsilon^2} \sum_{\substack{j \in K \cup K_\epsilon, \\ j \neq i}} f'(0)\left(\hat{u}_{l,j}^\epsilon(t) - \hat{u}_{l,i}^\epsilon(t)\right) \int_{x_i-\epsilon}^{x_i+\epsilon} \frac{\phi_j(y)J(|y - x_i|/\epsilon)}{|y - x_i|} dy + b_i(t), \tag{14}$$

with initial conditions (see Equation (12)) and boundary conditions (see Equation (13)).

We now write Equation (14) in vector form, and in the next section, we will use this representation to provide an explicit stability constraint on time step and mesh size for the linear peridynamic evolution. Let $U_{l,h}(t) = (\hat{u}_{l,i}^\epsilon(t))_{i \in K}$ be the vector of the approximate solution evaluated at the nodes. Then, Equation (14) can be written as

$$\rho \ddot{U}_{l,h}(t) = A U_{l,h}(t) + B(t), \tag{15}$$

where a_{ij} are defined as

$$a_{ij} = \begin{cases} \bar{a}_{ij}, & \text{if } j \neq i, \\ -\sum_{\substack{k \neq i, \\ k \in K \cup K_\epsilon}} \bar{a}_{ik}, & \text{if } j = i, \end{cases} \tag{16}$$

where

$$\bar{a}_{ij} = \frac{2}{\epsilon^2} f'(0) \int_{x_i-\epsilon}^{x_i+\epsilon} \frac{\phi_j(y)J(|y - x_i|/\epsilon)}{|y - x_i|} dy. \tag{17}$$

$B(t) = (b_i(t))_{i \in K}$ is the body force vector with

$$b_i(t) = b(t, x_i).$$

We point out that nonzero nonlocal boundary conditions can be prescribed on ∂D^ϵ. To do this, use the standard approach and include the known displacements corresponding to the nonlocal boundary K_ϵ on the right-hand side vector according to the rule

$$b_i(t) = b(t, x_i) + \sum_{j \in K_\epsilon, j \neq i} \bar{a}_{ij} \hat{u}_{l,j}^\epsilon.$$

To fix ideas, we first use linear continuous interpolation functions $\phi_i(x)$.

Linear continuous interpolation: Let $i \in K \cup K_\epsilon$. We define $\phi_i(x)$ as follows:

$$\phi_i(x) = \begin{cases} 0, & \text{if } x \notin [x_{i-1}, x_{i+1}], \\ \frac{x - x_{i-1}}{h}, & \text{if } x \in [x_{i-1}, x_i], \\ \frac{x_{i+1} - x}{h}, & \text{if } x \in [x_i, x_{i+1}], \end{cases}$$

with $x_{i+1} - x_i = h$, $i \in K \cup K_\epsilon$ and

$$\sum_{i \in K \cup K_\epsilon} \phi_i = 1,$$

and for $g \in C^2(\overline{D})$, we have

$$|\mathcal{I}_h[g(x)] - g(x)| \leq \sup_z \left| g''(z) \right| h^2.$$

3.1 | Consistency error

We present bounds on the consistency error due to discretization for both the nonlinear peridynamic force and the linearized peridynamic force. The error is seen to depend on the ratio of mesh size to nonlocality, ie, h/ϵ. The numerical examples given in Section 5 for both linear and nonlinear nonlocal models corroborate this trend.

h-convergence: We keep ϵ fixed and estimate the error with respect to mesh size h.

Proposition 2. (Consistency error: peridynamic approximation)
For linear continuous interpolation, if $u \in C^3(D)$ and u_{xxx} is bounded on D, then, for linearized peridynamic force, we have

$$\sup_{i \in K} \left| \nabla PD_l^\epsilon (\mathcal{I}_h[u])(x_i) - \nabla PD_l^\epsilon(u)(x_i) \right| = O(h/\epsilon), \tag{18}$$

and for the nonlinear peridynamic force, we have

$$\sup_{i \in K} |\nabla PD^\epsilon (\mathcal{I}_h[u])(x_i) - \nabla PD^\epsilon(u)(x_i)| = O(h/\epsilon). \tag{19}$$

We now examine what happens as ϵ goes to zero. Combining Propositions 1 and 2 and applying the triangle inequality gives the following.

Proposition 3. (Consistency error: peridynamic approximation in the limit $\epsilon \to 0$)
For linear continuous interpolation, if $u \in C^3(D)$ with u_{xxx} bounded, then, for the linearized peridynamic force, we have

$$\sup_{i \in K} \left| -\nabla PD_l^\epsilon (\mathcal{I}_h[u])(x_i) - \mathbb{C}u_{xx}(x_i) \right| = O(\epsilon) + O(h/\epsilon), \tag{20}$$

and for the nonlinear peridynamic force, we have

$$\sup_{i \in K} |-\nabla PD^\epsilon (\mathcal{I}_h[u])(x_i) - \mathbb{C}u_{xx}(x_i)| = O(\epsilon) + O(h/\epsilon). \tag{21}$$

This proposition shows that the consistency error for both nonlinear and linearized nonlocal models is controlled by the ratio of the mesh size to the horizon. This ratio must decrease to zero as the horizon goes to zero in order for the consistency error to go to zero. We conclude pointing out that the linearized kernels treaded in this work are different than those ones considered in the work of Tian and Du.[34]

3.2 | Consistency error for higher-order interpolation approximation

It is easy to improve the convergence results if we assume more differentiability for the solution. We will assume that we have uniform control of $p + 1$ bounded derivatives of solutions with respect to ϵ and discretize using higher-order local Lagrangian shape functions. In this section, we estimate the consistency error for this case. Let h be the mesh size and p be the order of interpolation. The discretization of the domain is now $D_h = D \cap (h/p)\mathbb{Z}$ and $\partial D^{\epsilon,h} = \partial D^\epsilon \cap (h/p)\mathbb{Z}$. Let $K := \{i \in \mathbb{Z} : i(h/p) \in \bar{D}\}$ and $K^\epsilon := \{i \in \mathbb{Z} : i(h/p) \in \partial \bar{D}^\epsilon\}$. The mesh points are denoted by $x_i = ih/p$, the interpolation operator is denoted by $\mathcal{I}_h[\cdot]$, and the extension operator is denoted by $E[\cdot]$. The approximate nonlinear peridynamic equation (11)

and approximate linearized peridynamic equation (14) are now defined for the pth order interpolations $\{\phi_i\}$. We now state the following results.

Proposition 4. (Consistency error: peridynamic approximation)
For continuous interpolation of order p, if $u \in C^{p+1}(D)$ and the $(p + 1)$th derivative of u is bounded on D, then, for the linearized peridynamic force, we have

$$\sup_{i \in K} \left| \nabla PD_l^\epsilon (\mathcal{I}_h[u])(x_i) - \nabla PD_l^\epsilon(u)(x_i) \right| = O(h^p/\epsilon), \tag{22}$$

and for the nonlinear peridynamic force, we have

$$\sup_{i \in K} | \nabla PD^\epsilon (\mathcal{I}_h[u])(x_i) - \nabla PD^\epsilon(u)(x_i) | = O(h^p/\epsilon). \tag{23}$$

Next, we examine what happens as we send ϵ to zero. Combining Propositions 1 and 4 and applying the triangle inequality gives the following.

Proposition 5. (Consistency error: peridynamic approximation in the limit $\epsilon \to 0$)
For continuous interpolation of order p, if $u \in C^{p+1}(D)$ with $(p + 1)$th derivative of u bounded, then, for the linearized peridynamic force, we have

$$\sup_{i \in K} \left| -\nabla PD_l^\epsilon (\mathcal{I}_h[u])(x_i) - \mathbb{C} u_{xx}(x_i) \right| = O(\epsilon) + O(h^p/\epsilon), \tag{24}$$

and for the nonlinear peridynamic force, we have

$$\sup_{i \in K} | -\nabla PD^\epsilon (\mathcal{I}_h[u])(x_i) - \mathbb{C} u_{xx}(x_i) | = O(\epsilon) + O(h^p/\epsilon). \tag{25}$$

Let $\bar{p} = \max\{p + 1, 4\}$. In case of linear peridynamics and $u \in C^{\bar{p}}(D)$ such that $\bar{p}$th derivative of u is bounded, we have

$$\sup_{i \in K} \left| -\nabla PD_l^\epsilon (\mathcal{I}_h[u])(x_i) - \mathbb{C} u_{xx}(x_i) \right| = O(\epsilon^2) + O(h^p/\epsilon). \tag{26}$$

For $p = 1$, we need $u \in C^3(D)$ (see Proposition 3). The outlines of proofs are provided in Section 7.

4 | THE CENTRAL DIFFERENCE SCHEME AND STABILITY ANALYSIS

In this section, we consider the central difference time discretization of the semidiscrete peridynamic equation (11). We recover a new stability condition for the linearized peridynamic equation, see Equation (28). An explicit stability condition relating Δt to h is obtained in terms of the linearized peridynamic material parameters. It is similar to the standard CFL condition for central difference approximation of 1D wave equation. We point out that the stability of the linearized peridynamic solution can imply the stability of nonlinear peridynamic solution. This implication is physically reasonable provided that the acceleration and body force are sufficiently small and so that one can approximate nonlinear peridynamics by its linearization.

Let Δt be the time step and the field $u(t)$ at time step $k \Delta t$ is denoted by u^k. To illustrate ideas, we will assume $\rho = 1$. For the linearized peridynamics, we characterize the matrix A associated with the spatial discretization equation (15). We introduce a special class of matrices.

Definition 1. An M matrix has negative off-diagonal elements m_{ij}, $i \neq j$, and the diagonal elements satisfy $m_{ii} \geq \sum_{j \neq i} m_{ij}$ for all i.

The stability of the numerical scheme is based on the following property of A.

Lemma 1. (Properties of A matrix)
For linear interpolations, the square matrix $-A$ of size $|K| \times |K|$ is a Stieltjes matrix, ie, it is a nonsingular symmetric M matrix. Therefore, the eigenvalues of $-A$ of is real and positive.

Proof. $-A$ is clearly M matrix as its off-diagonal terms are negative, and diagonal terms satisfy $-a_{ii} \geq \sum_{j \neq i} -a_{ij}$ for all i. To prove that an M matrix is nonsingular, we apply theorem 2.3 in chapter 6 in the work of Abraham and

Plemmons.[36] From the definition of $-A$, we find that

$$-a_{ii} = \sum_{i \neq j} -a_{ij}, \ i = 1, \ldots, n, \ -a_{ii} > \sum_{j=1}^{i-1} -a_{ij}, \ i = 2, \ldots, n,$$

and this is easily seen to be condition M_{37} of theorem 2.3 and we conclude that $-A$ is nonsingular. The symmetry of $-A$ is a straightforward consequence of formula (17). □

Central difference time discretization: For $\rho = 1$, the spatially discretized evolution equations for linearized peridynamics given by Equation (15) are written as

$$\ddot{U}_{l,h}(t) = AU_{l,h}(t) + B(t).$$

We now additionally discretize in time using the central difference scheme. Let $U_{l,h}^k := \{\hat{u}_{l,i}^{\epsilon,k}\}_{i \in K}$ denote the discrete displacement field at time step k. Here, we use the subscript "l" for linear peridynamic and superscript "ϵ" to highlight that the solution corresponds to size of horizon ϵ. In what follows, we will assume that no body force and the dynamics are driven by the initial conditions. Since we have the zero Dirichlet boundary condition, we know that the displacement at nodes $i \in K_\epsilon$ is zero for all time steps. We assume $k \leq T/\Delta t$, and the horizon is given by $\epsilon = mh/2$, where m is a positive integer. The discretized dynamics is given by the solution $\{U_{l,h}^k\}$ of the following equation:

$$\frac{U_{l,h}^{k+1} - 2U_{l,h}^k + U_{l,h}^{k-1}}{\Delta t^2} = AU_{l,h}^k,$$

or after elementary manipulation

$$U_{l,h}^{k+1} = -U_{l,h}^{k-1} + (2 + \Delta t^2 A)U_{l,h}^k. \tag{27}$$

Theorem 3. (Stability criterion for the central difference scheme)
Recall the elastic constant $\mathbb{C}$ given by Equation (2), $f'(0)$ given by Equation (1), and $M = \max_{0<r\leq 1}\{J(r)\}$. Then, the central difference scheme equation (27), in the absence of body forces, is stable as long as Δt satisfies

$$\Delta t \leq \frac{h}{\sqrt{\mathbb{C} + 2f'(0)\frac{Mh^2}{\epsilon^2}}}. \tag{28}$$

Remark. The stability condition for the linear elastic wave equation is given by the CFL condition $\Delta t \leq \frac{h}{\sqrt{\mathbb{C}}}$, where h gives the distance between mesh points.

Proof. Let (γ_i, v_i) be an eigenpair of A. Let $\lambda_i = -\gamma_i$, then $\lambda_i > 0$, and let $\lambda = \max_i\{\lambda_i\}$. Substitute $U_{l,h}^k = \xi^k v$, where ξ is some real number, and by ξ^k, we mean the kth power of ξ, into Equation (27), to obtain the characteristic equation

$$\xi^2 - 2\theta\xi + 1 = 0,$$

where $\theta = 1 - 1/2\lambda_i \Delta t^2$. The solution of the quadratic equation gives two roots: $\delta_1 = \theta + \sqrt{\theta^2 - 1}$ and $\delta_2 = \theta - \sqrt{\theta^2 - 1}$. We need $|\delta| \leq 1$ for stability. Since $\delta_1 \delta_2 = 1$, the only possibility is when $|\delta_1| = |\delta_2| = 1$. This is satisfied for all eigenmodes when

$$|\theta| \leq 1$$
$$\Rightarrow \Delta t \leq \frac{2}{\sqrt{\lambda}} \leq \frac{2}{\sqrt{\lambda_i}}.$$

A lower estimate on $1/\sqrt{\lambda}$ follows from Gershgorin's circle theorem.

Theorem 4. *Any eigenvalue of A lies inside at least one of the disks*

$$|\gamma - a_{ii}| < \sum_{i \neq j} |a_{ij}|. \tag{29}$$

All eigenvalues of A lie on the negative real axis, and we provide an upper estimate on the largest magnitude of the eigenvalues depending only on the mesh size h given by the distance between interpolation points and the horizon $\epsilon = mh$. For this case, it follows from Equations (29) and (16) that

$$\lambda < 2 \sum_{i \neq j} \overline{a}_{ij}.$$

Writing out the sum and using the definition of the interpolating functions and their partition of unity properties, we get

$$\sum_{i \neq j} \overline{a}_{ij} = \frac{2f'(0)}{\epsilon^2} \int_{x_{i-1}}^{x_{i+1}} \frac{1}{h} J(|y - x_i|/\epsilon) \, dy$$

$$+ \frac{2f'(0)}{\epsilon^2} \int_{x_i - \epsilon}^{x_{i-1}} \frac{J(|y - x_i|/\epsilon)}{|y - x_i|} \, dy$$

$$+ \frac{2f'(0)}{\epsilon^2} \int_{x_{i+1}}^{x_i + \epsilon} \frac{J(|y - x_i|/\epsilon)}{|y - x_i|} \, dy.$$

Here, we make use of the identities

$$1 = \sum_{j \in I^+} \phi^j(y), \ y \in [x_{i+1}, x_i + \epsilon],$$

$$1 = \sum_{j \in I^-} \phi^j(y), \ y \in [x_i - \epsilon, x_{i-1}],$$

where $I^+ = \{j : x_j \in [x_{i+1}, x_i + \epsilon]\}$ and $I^- = \{j : x_j \in [x_i - \epsilon, x_{i-1}]\}$. For $y < x_{i-1}$ and $x_{i+1} < y$, we have $h < |y - x_i|$ and $1 < |y - x_i|/h$ and we have the estimate

$$\sum_{i \neq j} \overline{a}_{ij} \leq 2\frac{\mathbb{C}}{h^2} + \frac{2f'(0)}{h\epsilon^2} \int_{x_{i-1}}^{x_{i+1}} J(|y - x_i|/\epsilon) \, dy$$

$$\leq 2\frac{\mathbb{C}}{h^2} + \frac{4}{\epsilon^2} f'(0)M,$$

and a lower bound now follows on $1/\sqrt{\lambda}$. Simple manipulation then delivers Equation (28). □

5 | NUMERICAL SIMULATION

In this section, we present numerical simulations that independently corroborate the theoretical bounds on the consistency error given in Section 3.1. We start in Section 5.1 and pose the nondimensional initial boundary value problem. We then perform a numerical study of the h-convergence in Section 5.2 and the convergence with respect to the ratio h/ϵ in Section 5.3. We compare the numerical simulations for the nonlinear and linear nonlocal models with local linear elastodynamics.

5.1 | Nondimensional peridynamic equation

Let $[0, L]$ be the bar with length L in meters. Let $[0, T]$ be the time domain in units of seconds. Given a dimensionless influence function $J(r)$, $r \in [0, 1]$, the bond force $f'(0)$ is in the units of N/m^2, and the density ρ in units of kg/m^3, the wave velocity in an equivalent linear elastic medium can be determined by

$$v_0 = \sqrt{f'(0)M/\rho}, \quad M := 2 \int_0^1 J(r)r \, dr.$$

We introduce the time scale $T_0 := L/v_0$. Then, a wave in the elastic media with elastic constant $\mathbb{C} = Mf'(0)$ requires T_0 seconds to reach from one end of the bar to the other end.

We let $\bar{x} = x/L$ for $x \in [0, L]$, and $\bar{t} = t/T_0$. We define nondimensional solution $\bar{u}(\bar{x}, \bar{t}) := u(L\bar{x}, T_0\bar{t})/L$. Let $\bar{\epsilon} := \epsilon/L$ be nondimensional size of horizon. Then, $\bar{u}$ satisfies

$$\ddot{\bar{u}}(\bar{t}, \bar{x}) = \frac{2}{\bar{\epsilon}^2} \int_{\bar{x}-\bar{\epsilon}}^{\bar{x}+\bar{\epsilon}} \bar{f}' \left(|\bar{y} - \bar{x}|\bar{S}^2\right) \bar{S}(\bar{y}, \bar{x}) J(|\bar{y} - \bar{x}|/\bar{\epsilon}) \mathrm{d}\bar{y} + \bar{b}(\bar{t}, \bar{x}),$$

where $\bar{S}(\bar{y}, \bar{x}; \bar{u}(\bar{t})) = (\bar{u}(\bar{t}, \bar{y}) - \bar{u}(\bar{t}, \bar{x}))/|\bar{y} - \bar{x}|$, $\bar{f}'(r) = \frac{L}{C} f'(Lr)$, and $\bar{b}(\bar{t}, \bar{x}) = \frac{L}{C} b(T_0\bar{t}, L\bar{x})$. The time interval T_0 for a given $E = f'(0)$ is given by $T_0 = L\sqrt{\rho/EM}$ and $u(t) = L\bar{u}(t/T_0)$.

In the following studies, we choose the influence function to be $J(|x|) = 2|x| \exp(-|x|^2/\alpha)$ with $\alpha = 0.4$. The nonlinear potential function f is taken to be $f(|x|S^2) = C(1 - \exp[-b|x|S^2])$. We let $b = 1$ and $f'(0) = Cb = C = 1/M$, where $M = 2\int_0^1 J(r)\mathrm{d}r$. This gives $T_0 = 1$. The body force is set to zero, ie, $b = 0$. All numerical results shown in this article will correspond to aforementioned choice of J, b, and f.

5.2 | *h*-convergence

We study the rate of convergence as seen in the simulations for two different choices of initial conditions. In the first problem, we consider the Gaussian pulse as the initial condition given by $u_0(x) = a \exp[-(0.5 - x)^2/\beta]$, $v_0(x) = 0.0$ with $a = 0.005$ and $\beta = 0.00001$. The time interval is $[0, 1.7]$ and the time step is $\Delta t = 0.00001$. We fix ϵ to 0.1 and consider the mesh sizes $h = \{\epsilon/10, \epsilon/100, \epsilon/1000\}$. For the second problem, we consider the double Gaussian curve as initial condition $u_0(x) = a \exp[-(0.25 - x)^2/\beta] + a \exp[-(0.75 - x)^2/\beta]$, $v_0(x) = 0.0$ with $a = 0.005$ and $\beta = 0.00001$. The time interval for the second problem is $[0, 0.5]$ and the time step is $\Delta t = 0.000005$. Here, we consider a smaller horizon $\epsilon = 0.01$ and solve for the three mesh sizes $h = \{\epsilon/100, \epsilon/200, \epsilon/400\}$.

Using the approximate solutions corresponding to three different mesh sizes, we can easily compute the dependence of the error with respect to mesh size h. Let u_1, u_2, and u_3 correspond to meshes of size h_1, h_2, and h_3, and let u be the exact solution. We write the error as $||u_h - u|| = Ch^\alpha$ for some constant C and $\alpha > 0$ and fix the ratio of mesh size $h_1/h_2 = h_2/h_3 = r$ to get

$$\log(||u_1 - u_2||) = C + \alpha \log h_2,$$
$$\log(||u_2 - u_3||) = C + \alpha \log h_3.$$

Then, the rate of convergence α is

$$\frac{\log(||u_1 - u_2||) - \log(||u_2 - u_3||)}{\log(r)}.$$

In Tables 1 and 2, we list the lower bound on the rate of convergence for different times in the evolution. The rate of convergence for the simulation is seen to depend on the time. We also note that the rate of convergence for the linear peridynamic solution is very close to that of the nonlinear peridynamic solution and both convergence rates lie above the theoretically predicted convergence rate for the L^2 error given by $\alpha = 1$.

5.3 | Convergence with respect to *h* and *h*/ε

We consider the limit of the peridynamic solution as $\epsilon \to 0$. The initial displacement is $u_0(x) = a \exp[-(0.5 - x)^2/\beta]$, $v_0(x) = 0.0$ with $a = 0.005$ and $\beta = 0.00001$. The time domain is taken to be $[0, 0.1]$ and the time step is $\Delta t = 0.0000005$. We fix the ratio $\epsilon/h = 100$ and solve the problem for three different peridynamic horizons given by $\epsilon = 0.0016$, $\epsilon = 0.0008$,

TABLE 1 Convergence result for problem 1. Superscript 1 refers to L^2 norm and 2 refers to sup norm. NPD refers to nonlinear peridynamic and LPD refers to linear peridynamic. Max time step is 170 000

Time Step	LPD[1]	NPD[1]	LPD[2]	NPD[2]
6 000	1.6416	1.6419	1.4204	1.4204
51 500	1.3098	1.3106	1.3312	1.3331
104 000	1.1504	1.1482	1.5155	1.5557
147 000	1.1364	1.1262	1.6027	1.5215
165 000	1.2611	1.2632	1.5496	1.6055

TABLE 2 Convergence result for problem 2. Superscript 1 refers to L^2 norm and 2 refers to sup norm. NPD refers to nonlinear peridynamic and LPD refers to linear peridynamic. Max time step is 10^5

Time Step	LPD^1	NPD^1	LPD^2	NPD^2
2 000	1.4498	1.4504	1.2546	1.2547
54 000	1.3718	1.3707	1.6903	1.6908
96 000	1.3735	1.3719	1.3753	1.3816

TABLE 3 Rate of convergence $\frac{\log(||u_1^\epsilon - u^{\epsilon_2}||) - \log(||u_2^\epsilon - u^{\epsilon_3}||)}{\log(\epsilon_2) - \log(\epsilon_3)}$

Time Step	Conv of LPD		Conv of NPD	
	L^2	sup	L^2	sup
2 000	1.9052	1.5556	1.9052	1.5556
50 000	1.7916	1.6275	1.7916	1.6275
100 000	1.718	1.449	1.718	1.449
150 000	1.6298	1.2688	1.6298	1.2688
200 000	1.5388	1.1086	1.5388	1.1086

Abbreviations: LPD, linear peridynamic; NDP, nonlinear peridynamic.

and $\epsilon = 0.0004$. As before, we assume a convergence error $||u^\epsilon - u|| \leq C\epsilon^\alpha$. The rate is of convergence in the simulations is measured by

$$\frac{\log(||u^{\epsilon_1} - u^{\epsilon_2}||) - \log(||u^{\epsilon_2} - u^{\epsilon_3}||)}{\log(\epsilon_2) - \log(\epsilon_3)}.$$

In Table 3, we record the convergence rate with respect to ϵ for different times in the evolution.

Comparison with the elastodynamic solution: Next, we compare the numerical solutions of elastodynamics, linear peridynamics, and nonlinear peridynamics. The comparison is made using the common initial data: $u_0(x) = a \exp[-(0.25 - x)^2/\beta] + a \exp[-(0.75 - x)^2/\beta]$, $v_0(x) = 0.0$ with $a = 0.001$ and $\beta = 0.003$. The time interval for simulation is $[0, 1.0]$ and the time step is $\Delta t = 0.000001$. The time interval has been chosen sufficiently large to include the effect of wave reflection off the boundary. In Figure 4, we plot the error $||u_{\text{peri}} - u_{\text{elasto}}||$ at each time step. Figure 4 validates the fact that the error depends on h/ϵ (see Equations (21) and (20)). In Figure 5, we plot the solutions at different time steps.

In Figure 4, we see that the error has a jump when t is close to $0.25, 0.5, 0.75, 0.95$. The jump near $t = 0.25$ and $t = 0.75$ is due to the wave dispersion effect when the wave hits the boundary. The reason for this is that for peridynamic simulations with smaller ϵ (compare green, cyan, and black curve in Figure 4 with that of large ϵ in blue, red, and yellow curve), the jump in error near $t = 0.25$ and $t = 0.75$ goes away irrespective of the h/ϵ ratio. As for the jump in error near $t = 0.5$ and $t = 0.95$, we look at the simulation and find that close to time $t = 0.5, 0.95$, there is an interaction between two Gaussian pulses traveling toward each other. This interaction is well captured by peridynamic solution when ϵ is small along with a small ratio h/ϵ. The cyan curve corresponds to smaller ϵ as compared with the blue curve. However, the jump near $t = 0.5$ and $t = 0.95$ does not improve much in the cyan curve. However, when we consider the finer mesh used in the simulation corresponding to the black curve with ϵ same as that of the cyan curve, the jump is greatly reduced.

The difference between the red and blue curves in Figure 5 at $t = 0.25$ and $t = 0.75$ is due to the presence of wave dispersion in the nonlocal model and reflection of the pulses by the boundary as described in Figure 4. The difference in red and blue curves at $t = 0.5$ and $t = 1.0$ is due to the interaction between the pulses as they approach each other and associated approximation error for the nonlocal model described in Figure 4.

Comparison between nonlinear and linear peridynamic solutions: In Proposition 1, we have shown that difference between the nonlinear and linearized peridynamic force is controlled by ϵ when the solution is smooth. Therefore, we would expect that, as the size of horizon gets smaller, the difference between approximate solution of linear and nonlinear peridynamics will get smaller. Let u_l^1, u_l^2 be the linear peridynamic solution and u^1, u^2 be the nonlinear peridynamic solution. "1" corresponds to ($\epsilon_1 = 0.01, h_1 = \epsilon/50$) and "2" ($\epsilon_2 = 0.005, h_2 = \epsilon/100$). Figure 6 shows the plot of slope $\frac{\log(||u^1 - u_l^1||_{L^2}) - \log(||u^2 - u_l^2||_{L^2})}{\log(\epsilon_1) - \log(\epsilon_2)}$ at different time steps. We see from the figure that the rate of convergence is very consistent with respect to time and is very close to expected value 1.
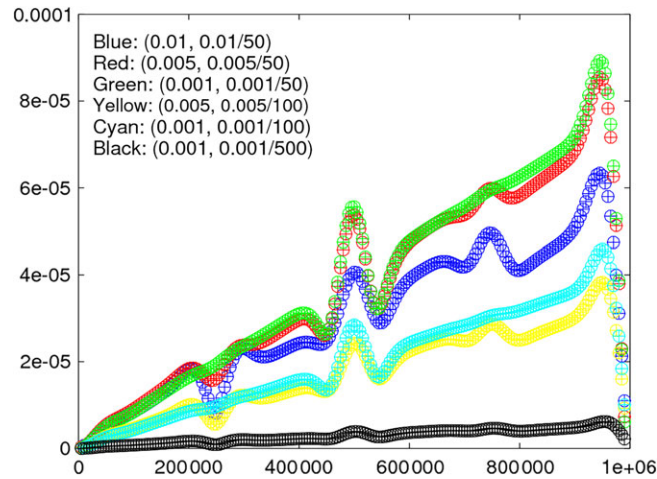
FIGURE 4 Plot of $||u_{\text{peri}} - u_{\text{elasto}}||_{L^2}$ at different time steps. Arguments inside the bracket corresponds to (ϵ, h). "+" corresponds to the linear peridynamics and "o" corresponds to nonlinear peridynamics. For $(\epsilon = 0.005, h = \epsilon/100)$ (yellow curve), the error $||u_{\text{peri}} - u_{\text{elasto}}||$ is smaller compared with the error for $(\epsilon = 0.01, h = \epsilon/50)$ (blue curve), whereas for the same $\epsilon = 0.005$ but with $h = \epsilon/50$ (red curve), the error is in fact higher than the error corresponding to $(\epsilon = 0.01, h = \epsilon/50)$ (blue curve). To further demonstrate the dependence of $||u_{\text{peri}} - u_{\text{elasto}}||$ on h/ϵ, the solution corresponding to $(\epsilon = 0.001, h = \epsilon/100)$ (cyan curve) lies above the yellow curve. However, when the ratio ϵ/h is increased to 500 (black curve), ie, for $(\epsilon = 0.001, h = \epsilon/500)$, we see that the black curve is lower than the yellow curve. Also note that the error plot corresponding to linear and nonlinear peridynamics is almost same ("+" and "o" overlap in each curve) [Colour figure can be viewed at wileyonlinelibrary.com]
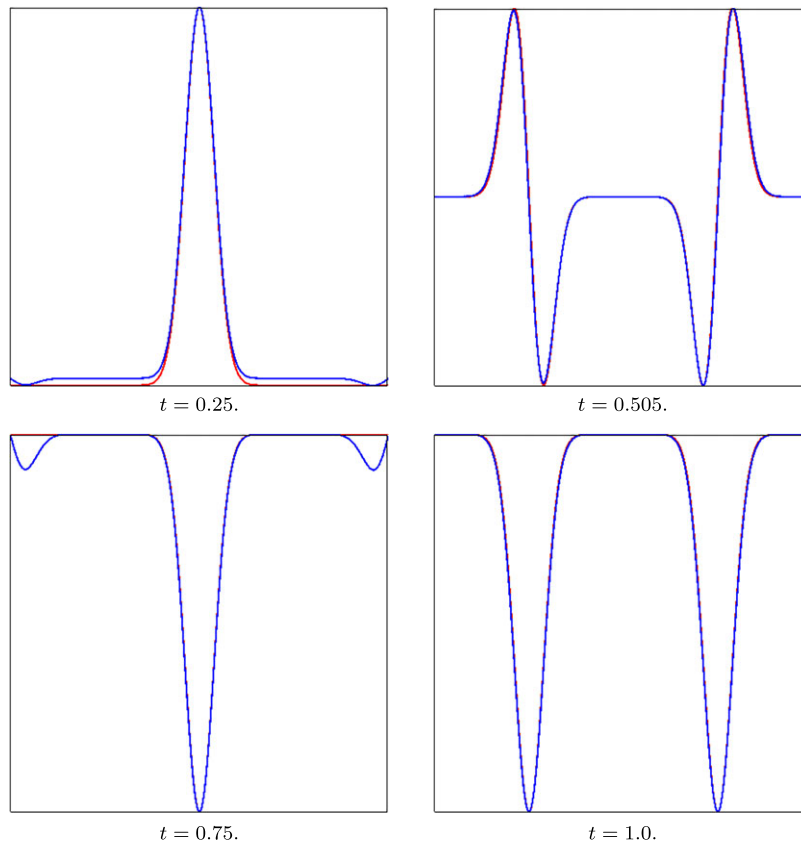
FIGURE 5 The elastodynamic solution is shown in red, linear peridynamics in green, and nonlinear peridynamics in blue. Simulation shows that solutions of linear and nonlinear peridynamics are nearly identical. The green curve is hidden beneath blue curve. The elastodynamic solution corresponds to mesh size $h = 0.00001$, whereas the peridynamic solution corresponds to $\epsilon = 0.005$ and $h = \epsilon/100$. Plots above are normalized so that the displacement lies within $[0, 1]$ [Colour figure can be viewed at wileyonlinelibrary.com]
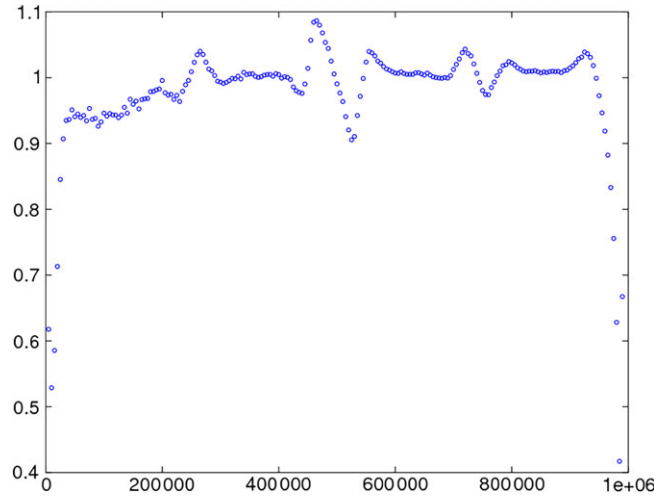
FIGURE 6 Slope of $\log(||u_{\mathrm{NPD}} - u_{\mathrm{LPD}}||_{L^2})$ with respect to $\log(\epsilon)$ at different time steps from $k = 0$ to $k = 10^6$ [Colour figure can be viewed at wileyonlinelibrary.com]

6 | CONVERGENCE OF NONLINEAR NONLOCAL MODELS TO LOCAL ELASTODYNAMICS IN DIMENSIONS 2 AND 3

We display the convergence of the nonlinear nonlocal model to elastodynamics in dimensions 2 and 3. In general, for $d = 1, 2, 3$, the nonlinear nonlocal force is given by

$$-\boldsymbol{\nabla} PD^\epsilon(u)(x) = \frac{4}{\epsilon^{d+1}\omega_d} \int\limits_{H_\epsilon(x)} J(|y-x|/\epsilon) f'\left(|y-x|S(y,x;u)^2\right) S(y,x;u)e_{y-x}\mathrm{d}y,$$

where $u \in L^2(D; \mathbb{R}^d)$, $H_\epsilon(x)$ is the ball of radius ϵ centered at x in $\mathbb{R}^d$, ω_d is the volume of unit ball in $\mathbb{R}^d$, $e_{y-x} = \frac{y-x}{|y-x|}$, and J and f are the same as before.

Proposition 6. (Control on the difference between peridynamic force and elastic force)
Let D be a bounded domain in $\mathbb{R}^d$. If $u \in C^3(D; \mathbb{R}^d)$ and $\sup_{x \in D}|\boldsymbol{\nabla}^3 u(x)| < \infty$, then

$$\sup_{x \in D}\left|-\boldsymbol{\nabla} PD^\epsilon(u)(x) - \boldsymbol{\nabla} \cdot \bar{\mathbb{C}}\mathcal{E}u(x)\right| = O(\epsilon),$$

where $\bar{\mathbb{C}}$ is given by

$$\bar{\mathbb{C}} = \frac{2f'(0)}{\omega_d} \int\limits_{H_1(0)} J(|\xi|)e_\xi \otimes e_\xi \otimes e_\xi \otimes e_\xi |\xi|\mathrm{d}\xi, \tag{30}$$

$e_\xi = \xi/|\xi|$ and the strain tensor is $\mathcal{E}u(x) = (\boldsymbol{\nabla}u(x) + \boldsymbol{\nabla}u^T(x))/2$.

In this treatment, we define the boundary ∂D of $D \subset \mathbb{R}^d$ in the usual way as the set of limit points of D. Similar to the case of one dimension, we consider $u = 0$ on ∂D and extend u by zero by zero outside D. We prescribe a nonlocal boundary condition on u^ϵ given by $u^\epsilon = 0$ on $\{x \in \mathbb{R}^d : \mathrm{dist}(x, \partial D) \leq \epsilon\}$. The initial conditions for u and u^ϵ are the same and given by u_0 and v_0 on D with u_0 and v_0 defined on $\mathbb{R}^d$, $d = 2, 3$ vanishing outside $D' \subset D$ such that $\mathrm{dist}(\partial D', \partial D) > 0$. We have the following.

Theorem 5. (Convergence of nonlinear peridynamics to the linear elastic wave equation in the limit that the horizon goes to zero)
Let $e^\epsilon := u^\epsilon - u$, where u^ϵ is the solution of peridynamics equation

$$\rho\ddot{u}^\epsilon(t,x) = -\boldsymbol{\nabla} PD^\epsilon(u^\epsilon(t))(x) + b(t,x), \tag{31}$$

and u is the solution of elastodynamics equation

$$\rho\ddot{u}(t,x) = \boldsymbol{\nabla} \cdot \bar{\mathbb{C}}\mathcal{E}u(t,x) + b(t,x), \tag{32}$$

with elastic tensor given by Equation (30). We assume that u^ϵ and u satisfy the same initial condition and $u = 0$ on ∂D. Suppose $u^\epsilon(t) \in C^4(D; \mathbb{R}^d)$, for all $\epsilon > 0$ and $t \in [0, T]$. Suppose there exists $C_1 > 0$, C_1 independent of the size of horizon ϵ, such that

$$\sup_{\epsilon > 0} \left[\sup_{(x,t) \in D \times J} \left| \nabla^4 u^\epsilon(t, x) \right| \right] < C_1 < \infty.$$

Then, for ϵ such that $\mathrm{dist}(\partial D', \partial D) > \epsilon > 0$, there exists $\exists C_2 > 0$ such that

$$\sup_{t \in [0,T]} \left\{ \int_D \rho |\dot{e}^\epsilon(t, x)|^2 \mathrm{d}x + \int_D \mathcal{E}e^\epsilon(t, x) \cdot \bar{\mathbb{C}}\mathcal{E}e^\epsilon(t, x) \mathrm{d}x \right\} \leq C_2 \epsilon^2,$$

so $u^\epsilon \to u$ in the $H^1(D; \mathbb{R}^d)$ norm at the rate ϵ uniformly in time $t \in [0, T]$.

The proof is similar to the case of one dimension except in this case where vector nature of displacement field has to be considered. Following the steps in Section 7, Proposition 6 and Theorem 5 can be shown, and therefore, we omit the proof.

7 | PROOF OF CLAIMS

In this section, we will present the proof of claims in Sections 2 and 3. For simplification, we adopt the following notation:

$$p := u_x(x), \qquad q := u_{xx}(x), \qquad r := u_{xxx}(x),$$

$$e := \frac{(y - x)}{|y - x|} = \mathrm{sign}\{y - x\}. \tag{33}$$

In proving results related to consistency error, we will employ the Taylor series expansion of $u(y)$ with respect to point x_i. Since the potential f is assumed to be sufficiently smooth, $f''(r)$, $f'''(r)$, and $f''''(r)$ are bounded for $0 < r < \infty$.

7.1 | Bound on difference of peridynamic, linear peridynamic, and elastodynamic force

We prove Proposition 1 for $u \in C^3(D)$. Using Taylor series expansion, we get

$$S(y, x; u) = u_x(x) \frac{y - x}{|y - x|} + 1/2 u_{xx}(x)|y - x| + 1/6 u_{xxx}(\xi)|y - x|(y - x)$$

$$= pe + q|y - x|/2 + T_1(y - x)/|y - x|,$$

where $T_1 = O(|y - x|^3)$. On taking the Taylor series expansion of the nonlinear potential and substituting in the aforementioned expansion, we get

$$\left(f'(|y - x| S(y, x; u)^2) - f'(0) \right) S(y, x; u) = f''(0) p^3 |y - x| e + (f''(0) p^2 q 3/2 + f'''(0) p^5 e/2)|y - x|^2 + T_2(y - x),$$

where $T_2(y - x) = O(|y - x|^3)$. Using the previous equation, we get

$$-\nabla PD^\epsilon(u)(x) + \nabla PD_l^\epsilon(u)(x)$$

$$= \frac{2}{\epsilon^2} \int_{x-\epsilon}^{x+\epsilon} J(|y - x|/\epsilon) \left(f'(|y - x| S(y, x; u)^2) - f'(0) \right) S(y, x; u) \mathrm{d}y$$

$$= \frac{2}{\epsilon^2} \int_{x-\epsilon}^{x+\epsilon} \left[f''(0) p^3 |y - x| e + \left(f''(0) p^2 q 3/2 + f'''(0) p^5 e/2 \right) |y - x|^2 + T_2(y - x) \right] J(|y - x|/\epsilon) \mathrm{d}y$$

$$= \frac{2}{\epsilon^2} \int_{x-\epsilon}^{x+\epsilon} f''(0) p^2 q 3/2 |y - x|^2 J(|y - x|/\epsilon) \mathrm{d}y + O(\epsilon^2)$$

$$= O(\epsilon),$$

where terms with e integrate to zero. From this, we see that same estimate holds when u has continuous and bounded third or fourth derivatives. This proves the assertion of Proposition 1.

To prove Equation (7), we proceed as follows:

$$-\nabla PD_l^\epsilon(u)(x) = \frac{2}{\epsilon^2} \int_{x-\epsilon}^{x+\epsilon} J(|y-x|/\epsilon) f'(0) S(y,x;u) \mathrm{d}y$$

$$= \frac{2}{\epsilon^2} \int_{x-\epsilon}^{x+\epsilon} J(|y-x|/\epsilon) f'(0) \left[pe + q|y-x|/2 + T_1(y-x)/|y-x| \right] \mathrm{d}y$$

$$= \left(\frac{2}{\epsilon^2} \int_{x-\epsilon}^{x+\epsilon} J(|y-x|/\epsilon) f'(0) |y-x|/2 \mathrm{d}y \right) q + O(\epsilon)$$

$$= \mathbb{C} u_{xx}(x) + O(\epsilon),$$

where we identify $\mathbb{C}$ using Equation (2), and $q = u_{xx}(x)$. This proves Equation (7).

To prove Equation (10), we assume $u \in C^4(D)$ and Equation (9). Then, by Taylor series expansion, we have

$$S(y,x;u) = u_x(x) \frac{y-x}{|y-x|} + 1/2 u_{xx}(x)|y-x|$$

$$+ 1/6 u_{xxx}(x)|y-x|(y-x) + 1/24 u_{xxxx}(\xi)|y-x|^3$$

$$= pe + q|y-x|/2 + r|y-x|^2 e + T_1(y-x)/|y-x|,$$

where $T_1(y-x) = O(|y-x|^4)$. Substituting this into $-\nabla PD_l^\epsilon(u)(x)$ and noting that terms with e integrate to zero, we get

$$-\nabla PD_l^\epsilon(u)(x) = \mathbb{C} u_{xx}(x) + O(\epsilon^2).$$

7.2 | Convergence of solution of peridynamic equation to the elastodynamic equation

To prove Theorem 1, we proceed as follows. Let u^ϵ be the solution of peridynamic model in Equation (4), and let u be the solution of elastodynamic equation in Equation (3). Boundary conditions and initial conditions are same as described in Section 2. Assuming that the hypothesis of Theorem 1 holds, we have from Proposition 1

$$-\nabla PD^\epsilon(u^\epsilon(t))(x) = \mathbb{C} u_{xx}^\epsilon(t,x) + O(\epsilon).$$

We have also assumed that there exists $C_1 < \infty$ such that

$$\sup_{\epsilon>0} \left[\sup_{(x,t)\in D\times J} |u_{xxxx}^\epsilon(t,x)| \right] < C_1 < \infty.$$

Combining this together with (8) we have,

$$\sup_{(x,t)\in D\times J} |-\nabla PD^\epsilon(u^\epsilon(t))(x) - \mathbb{C} u_{xx}^\epsilon(t,x)| \le C_3 \epsilon,$$

where C_3 is independent of x, t and ϵ. Subtracting equation (4) from equation (3) shows that $e^\epsilon = u^\epsilon - u$ satisfies

$$\rho \ddot{e}^\epsilon(t,x) = \mathbb{C} e_{xx}^\epsilon(t,x) + (-\nabla PD^\epsilon(u^\epsilon(t))(x) - \mathbb{C} u_{xx}^\epsilon(t,x))$$

$$= \mathbb{C} e_{xx}^\epsilon(t,x) + F(t,x), \tag{34}$$

where

$$F(t,x) = -\nabla PD^\epsilon(u^\epsilon(t))(x) - \mathbb{C} u_{xx}^\epsilon(t,x) \quad \text{and} \quad \sup_{(x,t)\in D\times J} |F(t,x)| \le C_3 \epsilon,$$

with boundary condition and initial condition given by

$$e^\epsilon(0,x) = 0, \quad \dot{e}^\epsilon(0,x) = 0 \qquad \forall x \in D,$$

$$e^\epsilon(t,x) = 0, \quad \dot{e}^\epsilon(t,x) = 0 \qquad \forall (t,x) \in [0,T] \times \partial D^\epsilon.$$

Since e^ϵ satisfies Equation (34) we can apply Gronwall's inequality to find

$$\sup_{t\in J} \int_D \rho |\dot{e}^\epsilon(t,x)|^2 \mathrm{d}x + \int_D \mathbb{C} |e_x^\epsilon(t,x)|^2 \mathrm{d}x \le C_2 \epsilon^2. \tag{35}$$

Now, to show that $e^\epsilon \to 0$ in $H^1(D)$, we apply Equation (35) together with Poincare's inequality to get

$$\|e^\epsilon(t,x)\|^2_{L^2(D)} \le C \|e^\epsilon_x(t,x)\|^2_{L^2(D)}$$

$$\le \frac{C}{\mathbb{C}} \sup_{t\in[0,T]} \left\{ \int_D \rho|\dot{e}^\epsilon(t,x)|^2 \mathrm{d}x + \int_D \mathbb{C}|e^\epsilon_x(t,x)|^2 \mathrm{d}x \right\}$$

$$\le \frac{C}{\mathbb{C}} C_2 \epsilon^2,$$

where C is the Poincare constant. On collecting results this shows that $e^\epsilon \to 0$ in the $H^1(D)$ norm with the rate ϵ. This completes the proof of Theorem 1. Identical arguments using Equation (10) deliver Theorem 2.

7.3 | Bounds on the consistency error

We first prove for linear continuous interpolation and then extend the proof to higher-order interpolations.

7.3.1 | Linear interpolation

In this section, Proposition 2 is established. We begin by writing the difference $S(y,x_i; \mathcal{I}_h[u]) - S(y,x_i; u)$. It is given by

$$S(y,x_i; \mathcal{I}_h[u]) - S(y,x_i; u) = \frac{\mathcal{I}_h[u](y) - u(y)}{|y - x_i|}. \tag{36}$$

From the hypothesis of Proposition 2, there is a constant C for which $|u_{xx}| < C$ on D. Using the approximation property $|\mathcal{I}_h[u] - u| \le Ch^2$ and applying $|y - x_i| > h$ for y outside the interval $[x_{i-1}, x_{i+1}]$ gives

$$|S(y,x_i; \mathcal{I}_h[u]) - S(y,x_i; u)| \le \begin{cases} C|y - x_i|, & \text{if } y \in [x_{i-1}, x_{i+1}], \\ Ch, & \text{if } y \in [x_i - \epsilon, x_{i-1}], \\ Ch, & \text{if } y \in [x_{i+1}, x_i + \epsilon]. \end{cases}$$

Note further that $|y - x_i| \le h$ for $y \in [x_{i-1}, x_{i+1}]$ and we conclude

$$|S(y,x_i; \mathcal{I}_h[u]) - S(y,x_i; u)| \le Ch. \tag{37}$$

Straightforward calculation shows

$$\left| \nabla PD^\epsilon_\ell (\mathcal{I}_h[u]) - \nabla PD^\epsilon_\ell(u) \right| \le \frac{2f'(0)}{\epsilon^2} \int_{x_i-\epsilon}^{x_i+\epsilon} |S(y,x_i, \mathcal{I}_h[u]) - S(y,x_i; u)| J(|y - x_i|/\epsilon) \mathrm{d}y$$

$$\le \frac{4f'(0)MCh}{\epsilon},$$

where $M = \max_{0 \le z < 1} J(z)$ and Equation (18) of Proposition 2 follows.

We now establish the consistency error for the nonlinear nonlocal model. We begin with an estimate for the strain. Applying the notation described in (33) with p and e defined for $x = x_i$, we apply Taylor's theorem with remainder to get

$$S(y,x_i; u) = u_x(x_i)(y - x_i)/|y - x_i| + u_{xx}(\xi)|y - x_i|/2$$
$$= pe + T_1(y - x_i)/|y - x_i|, \tag{38}$$

where $T_1(y - x_i) = O(|y - x_i|^2)$.

From Equation (37), we can write

$$S(y,x_i; u) = S(y,x_i; \mathcal{I}_h[u]) + O(h),$$

or

$$S(y,x_i; \mathcal{I}_h[u]) = S(y,x_i; u) + O(h), \tag{39}$$

or we can write $S(y, x_i; u) = S(y, x_i; \mathcal{I}_h[u]) + \eta$, where $|\eta| < Ch$. Adopting this convention, first we write

$$|y - x_i|S^2(y, x_i; u) = |y - x_i|(S(y, x_i; \mathcal{I}_h[u]) + \eta)^2$$
$$= |y - x_i|S^2(y, x_i; \mathcal{I}_h[u]) + \sum_{j \in I} 2\eta\phi_j(y)(u(x_j) - u(x_i)) + |y - x_i|\eta^2,$$

where the set $I = \{j : x_j \in [x_i - \epsilon, x_i + \epsilon]\}$ and we have used the identity

$$1 = \sum_{j \in I} \phi_j(y), y \in [x_i - \epsilon, x_i + \epsilon].$$

Next, we estimate

$$\sum_{j \in I} \phi_j(y)(u(x_j) - u(x_i)) \leq \sup\{|u(y) - u(x_i)| \text{ for } y \in [x_i - \epsilon, x_i + \epsilon]\}$$

$$\leq 2\epsilon \sup_{y \in D} |u_x(y)|.$$

Since u_x is bounded, we see that $\sum_{j \in I} \phi_j(y)(u(x_j) - u(x_i)) = \zeta$, where $|\zeta| \leq \epsilon\text{Const}$, and

$$|y - x_i|S^2(y, x_i; u) = |y - x_i|(S(y, x_i; \mathcal{I}_h[u])^2 + 2\zeta\eta + \eta^2$$

Applying Taylor's theorem with remainder to the function $f'(|y - x|(S(y, x_i; \mathcal{I}_h[u]) + \eta)^2)$ now gives

$$f'\left(|y - x|S(y, x_i; u)^2\right) = f'\left(|y - x|(S(y, x_i; \mathcal{I}_h[u]))^2\right) + O(h), \tag{40}$$

where we have used that $f''(r)$ is bounded on $0 \leq r \leq \infty$.

Then, application of Equations (38), (39), and (40) and substitution delivers the desired estimate

$$-\nabla PD^\epsilon(\mathcal{I}_h[u])(x_i) + \nabla PD^\epsilon(u)(x_i)$$

$$= \frac{2}{\epsilon^2} \int_{x_i-\epsilon}^{x_i+\epsilon} f'\left(|y - x|(S(y, x_i; \mathcal{I}_h[u]))^2\right)(S(y, x_i; u) + O(h))J(|y - x_i|/\epsilon)\mathrm{d}y$$

$$- \frac{2}{\epsilon^2} \int_{x_i-\epsilon}^{x_i+\epsilon} \left(f'\left(|y - x|(S(y, x_i; \mathcal{I}_h[u]))^2\right) + O(h)\right) S(y, x_i; u)J(|y - x_i|/\epsilon)\mathrm{d}y$$

$$= O(h/\epsilon),$$

and Equation (19) of Proposition 2 is proved.

7.3.2 | Higher-order interpolations and convergence

In this section, we outline the proof of higher-order accuracy using higher-order interpolation functions when the solution has sufficiently high-order bounded derivatives. The order of the interpolation is p, the mesh size h, and the grid points are $x_i = ih/p$ for $i \in K \cup K^\epsilon$. We state the following key result.

Lemma 2. *If $u \in C^{p+1}(D)$ with $(p + 1)$th derivative bounded, then, for pth-order interpolation, we have the following estimate:*

$$|S(y, x_i; \mathcal{I}_h[u]) - S(y, x_i; u)| \leq \tilde{C}h^p \qquad \forall i \in K, \forall y \in [x_i - \epsilon, x_i + \epsilon], \tag{41}$$

where constant $\tilde{C}$ is independent of h, i, and y.

Proof. Fix some $i \in K$. There exist $C > 0$ such that $\sup |\partial_x^{p+1}u| < C$. The interpolation error[37] is $|\mathcal{I}_h[u](y) - u(y)| \leq Ch^{p+1}$ for all $y \in \overline{D \cup \partial D^\epsilon}$. Now, for $y \in [x_i - \epsilon, x_{i-1}] \cup [x_{i+1}, x_i + \epsilon]$, $h \leq |y - x_i|$ and hence $\frac{1}{|y-x_i|} \leq \frac{1}{h}$. Thus, from Equation (36), we have

$$|S(y, x_i; \mathcal{I}_h[u]) - S(y, x_i; u)| \leq Ch^p. \tag{42}$$

$\square$

The proofs of Propositions 4 and 5 now follow using Lemma 2 and applying the same steps used in the proofs of Propositions 2 and 3 for linear interpolation.

8 | CONCLUSION

Earlier related work[25] analyzed the model considered here but for less regular nondifferentiable Hölder continuous solutions. For that case, solutions can approach discontinuous deformations (fracture-like solutions) as $\epsilon \to 0$ and it is shown that the numerical approximation of the nonlinear model in dimension $d = 1, 2, 3$ converges to the exact solution at the rate $O(\Delta t + h^\gamma/\epsilon^2)$, where $\gamma \in (0, 1]$ is the Hölder exponent, h is the size of mesh, ϵ is the size of horizon, and Δt is the size of time step. In this work, we have shown that we can improve the rate of convergence if we somehow have a priori knowledge on the number of bounded continuous derivatives of the solution. If the solution has $p + 1$ derivatives, one can use pth-order polynomial local interpolation and obtain an order h^p/ϵ consistency error.

In this work, we have analyzed the smooth prototypical micro-elastic bond model introduced in the work of Silling.[1] From the perspective of computation, the resolution of the mesh inside the horizon of nonlocal interaction is the main contributor to the computational complexity. This work provides explicit error estimates for the differences between the solutions of elastodynamics and nonlocal models. It shows that the effects of the mesh size relative to the horizon can be significant. Numerical errors can grow with decreasing horizon if the mesh is not chosen suitably small with respect to the peridynamic horizon. A fixed ratio of mesh size to horizon will not increase accuracy as the horizon tends to zero. We have carried out numerical simulations where the accuracy decreases when ϵ is reduced and the ratio h/ϵ is fixed. This is shown to be in line with the consistency error bounds that vanish at the rate $O(h/\epsilon)$. These results show that the grid refinement relative to the horizon length scale has more importance than decreasing the horizon length when establishing convergence to the classical elastodynamics description.

The results of this analysis rigorously show that one can use a discrete linear local elastodynamic model to approximate the nonlinear nonlocal evolution when sufficient regularity of the evolution is known a priori. In doing so, one incurs a modeling error of order ϵ but saves computational work in that there is no nonlocality so the mesh diameter h no longer has to be small relative to ϵ. The discretization error is now associated with the approximation error for the initial boundary value problem for the linear elastic wave equation.

We reiterate that the nonlinear kernel analyzed here corresponds to a smooth version of the prototypical micro-elastic bond model treated in the work of Silling.[1] On the other hand, its linearization corresponds to the one of the types kernel functions treated in the work of Chen et al.[38] In this paper, the goal is to understand the convergence of numerical schemes for the nonlinear model together with its linearization with respect to horizon and discretization. The work of Chen et al[38] asks distinctly different questions and is concerned with identifying linear nonlocal models that converge to linear elastodynamics when the mesh density is held fixed and the horizon of nonlocality goes to zero. This is not the case for the kernel treated here.

Our results and analysis support a combined local-nonlocal approach to the numerical solution of these problems. This type of numerical approach is the focus of many recent investigations, see other works,[39-46] where the use of nonlocal models and local models is applied to different subdomains of the computational domain. These approaches are promising in that they reduce the computational cost of the numerical simulation. A full understanding of the error associated in implementing these adaptive methods is an exciting prospect for future research.

ORCID

Prashant K. Jha http://orcid.org/0000-0003-2158-364X
Robert Lipton http://orcid.org/0000-0002-1382-3204

REFERENCES

1. Silling SA. Reformulation of elasticity theory for discontinuities and long-range forces. *J Mech Phys Solids*. 2000;48(1):175-209.
2. Silling SA, Weckner O, Askari E, Bobaru F. Crack nucleation in a peridynamic solid. *Int J Frac*. 2010;162(1-2):219-227.
3. Bobaru F, Hu W. The meaning, selection, and use of the peridynamic horizon and its relation to crack branching in brittle materials. *Int J Fract*. 2012;176(2):215-222.
4. Ha YD, Bobaru F. Studies of dynamic crack propagation and crack branching with peridynamics. *Int J Frac*. 2010;162(1-2):229-244.

5. Agwai A, Guven I, Madenci E. Predicting crack propagation with peridynamics: a comparative study. *Int J Fract*. 2011;171(1):65-78.

6. Ghajari M, Iannucci L, Curtis P. A peridynamic material model for the analysis of dynamic crack propagation in orthotropic media. *Comput Method Appl Mech Eng*. 2014;276:431-452.

7. Diehl P, Lipton R, Schweitzer MA. Numerical verification of a bond-based softening peridynamic model for small displacements: Deducing material parameters from classical linear theory. Bonn, Germany: Institut für Numerische Simulation, Rheinische Friedrich-Wilhelms-Universität Bonn; 2016.

8. Bobaru F, Yang M, Alves LF, Silling SA, Askari E, Xu J. Convergence, adaptive refinement, and scaling in 1D peridynamics. *Int J Numer Method Eng*. 2009;77(6):852-877.

9. Dayal K, Bhattacharya K. Kinetics of phase transformations in the peridynamic formulation of continuum mechanics. *J Mech Phys Solids*. 2006;54(9):1811-1842.

10. Foster JT, Silling SA, Chen W. An energy based failure criterion for use with peridynamic states. *Int J Multiscale Comput Eng*. 2011;9(6).

11. Ha YD, Bobaru F. Characteristics of dynamic brittle fracture captured with peridynamics. *Eng Frac Mech*. 2011;78(6):1156-1168.

12. Silling SA, Bobaru F. Peridynamic modeling of membranes and fibers. *Int J Non-Linear Mech*. 2005;40(2):395-409.

13. Weckner O, Abeyaratne R. The effect of long-range forces on the dynamics of a bar. *J Mech Phys Solids*. 2005;53(3):705-728.

14. Silling SA, Askari E. A meshfree method based on the peridynamic model of solid mechanics. *Comput Struct*. 2005;83(17):1526-1535.

15. Lipton R, Silling S, Lehoucq R. Complex fracture nucleation and evolution with nonlocal elastodynamics. arXiv preprint arXiv:1602.00247; 2016.

16. Weckner O, Emmrich E. Numerical simulation of the dynamics of a nonlocal, inhomogeneous, infinite bar. *J Comput Appl Mech*. 2005;6(2):311-319.

17. Silling SA, Lehoucq RB. Convergence of peridynamics to classical elasticity theory. *J Elasticity*. 2008;93(1):13-37.

18. Mengesha T, Du Q. Nonlocal constrained value problems for a linear peridynamic Navier equation. *J Elasticity*. 2014;116(1):27-51.

19. Tian X, Du Q, Gunzburger M. Asymptotically compatible schemes for the approximation of fractional Laplacian and related nonlocal diffusion problems on bounded domains. *Adv Comput Math*. 2016;42(6):1363-1380.

20. Chen X, Gunzburger M. Continuous and discontinuous finite element methods for a peridynamics model of mechanics. *Comput Method Appl Mech Eng*. 2011;200(9):1237-1250.

21. Du Q, Gunzburger M, Lehoucq RB, Zhou K. Analysis and approximation of nonlocal diffusion problems with volume constraints. *SIAM Rev*. 2012;54(4):667-696.

22. Guan Q, Gunzburger M. Stability and accuracy of time-stepping schemes and dispersion relations for a nonlocal wave equation. *Numer Method Partial Diff Equa*. 2015;31(2):500-516.

23. Lipton R. Dynamic brittle fracture as a small horizon limit of peridynamics. *J Elasticity*. 2014;117(1):21-50.

24. Lipton R. Cohesive dynamics and brittle fracture. *J Elasticity*. 2016;124(2):143-191.

25. Jha PK, Lipton R. Numerical analysis of peridynamic models in Hölder space. *SIAM J Numer Anal*. To appear 2018.

26. Mengesha T, Du Q. Analysis of a scalar peridynamic model with a sign changing kernel. *Discrete Contin Dyn Syst B*. 2013;18:1415-1437.

27. Du Q, Zhou K. Mathematical analysis for the peridynamic nonlocal continuum theory. *ESAIM: Math Model Numer Anal*. 2011;45(2):217-234.

28. Emmrich E, Lehoucq RB, Puhst D. Peridynamics: a nonlocal continuum theory. *Meshfree Methods for Partial Differential Equations VI*. Berlin, Germany: Springer; 2013:45-65.

29. Aksoylu B, Parks ML. Variational theory and domain decomposition for nonlocal problems. *Appl Math Comput*. 2011;217(14):6498-6515.

30. Aksoylu B, Unlu Z. Conditioning analysis of nonlocal integral operators in fractional Sobolev spaces. *SIAM J Numer Anal*. 2014;52(2):653-677.

31. Dayal K. Leading-order nonlocal kinetic energy in peridynamics for consistent energetics and wave dispersion. *J Mech Phys Solids*. 2017;105:235-253.

32. Florin B, Foster JT, Geubelle PH, Geubelle PH, Silling SA. *Handbook of Peridynamic Modeling*. Boca Raton, FL: CRC Press; 2016.

33. Emmrich E, Weckner O. On the well-posedness of the linear peridynamic model and its convergence towards the navier equation of linear elasticity. *Commun Math Sci*. 2007;5(4):851-864.

34. Tian X, Du Q. Analysis and comparison of different approximations to nonlocal diffusion and linear peridynamic equations. *SIAM J Numer Anal*. 2013;51(6):3458-3482.

35. Tian X, Du Q. Asymptotically compatible schemes and applications to robust discretization of nonlocal models. *SIAM J Numer Anal*. 2014;52(4):1641-1665.

36. Abraham B, Plemmons RJ. *Nonnegative Matrices in the Mathematical Sciences*. Classics in Applied Mathematics. vol 9. Philadelphia, PA: Society for Industrial and Applied Mathematics; 1987.

37. Isaacson E, Keller HB. *Analysis of Numerical Methods*. New York, NY: John Wiley & Sons; 1966.

38. Chen Z, Bakenhus D, Bobaru F. A constructive peridynamic kernel for elasticity. *Comput Method Appl Mech Eng*. 2016;311:356-373.

39. Wildman RA, Gazonas GA. A finite difference-augmented peridynamics method for reducing wave dispersion. *Int J Fract*. 2014;190(1-2):39-52.

40. Seleson P, Beneddine S, Prudhomme S. A force-based coupling scheme for peridynamics and classical elasticity. *Computat Mater Scie*. 2013;66:34-49.

41. Kilic B, Madenci E. Coupling of peridynamic theory and the finite element method. *J Mech Materials Struct*. 2010;5(5):707-733.

42. Oterkus E, Madenci E, Weckner O, Silling S, Bogert P, Tessler A. Combined finite element and peridynamic analyses for predicting failure in a stiffened composite curved panel with a central slot. *Compos Struct*. 2012;94(3):839-850.

43. Zaccariotto M, Tomasi D, Galvanetto U. An enhanced coupling of PD grids to FE meshes. *Mech Res Commun*. 2017;84:125-135.

44. Han F, Lubineau G, Azdoud Y, Askari A. A morphing approach to couple state-based peridynamics with classical continuum mechanics. *Comput Method Appl Mech Eng*. 2016;301:336-358.

45. Lubineau G, Azdoud Y, Han F, Rey C, Askari A. A morphing strategy to couple nonlocal to local continuum mechanics. *J Mech Phys Solids*. 2012;60(6):1088-1102.

46. Liu W, Hong J-W. A coupling approach of discretized peridynamics with finite element method. *Comput Method Appl Mech Eng*. 2012;245:163-175.